In depth analysis of Fourier-based wavefront sensors with the adaptive optics testbed LOOPS.

Pierre Janin-Potiron[a,b,*], Vincent Chambouleyron[a,b], Lauren Schatz[c,b], Olivier Fauvarque[b], Charlotte Z. Bond[d], Eduard Muslimov[b], Kacem El-Hadi[b], Jean-François Sauvage[a,b], Kjetil Dohlen[b], Benoît Neichel[b], Carlos M. Correia[b], Noëline Villard[b], Sofiane Aïssani[b], Mojtaba Taheri[e], and Thierry Fusco[a,b]

[a]ONERA The French Aerospace Laboratory, F-92322 Châtillon, France
[b]Aix Marseille Univ, CNRS, CNES, LAM, Marseille, France
[c]The University of Arizona, College of Optical Sciences, 1630 E University Blvd, Tucson, AZ 85719, USA
[d]Institute for Astronomy University of Hawaii-Manoa 640 N. Aohoku Place Hilo, HI 96720 USA
[e]University of Victoria, Canada

ABSTRACT

The development and study of new, more robust and powerful wavefront sensors plays an important role in the improvement of the wavefront sensing capabilities of adaptive optics systems. The LAM-ONERA On-sky Pyramid Sensor is a R&D bench dedicated to study and characterize these new wavefront sensors. In this paper, we give a glance at the current status of the bench in terms of hardware and at the most recent results obtained using new flavours of Fourier filtering wavefront sensors.

Keywords: adaptive optics, optical bench, pyramid wavefront sensor, Fourier-based wavefront sensors, spatial light modulator

1. INTRODUCTION

The LAM-ONERA On-sky Pyramid Sensor (LOOPS[1, 2]) is an adaptive optics facility hosted at Laboratoire d'Astrophysique de Marseille and focusing on the study of Fourier-filtering wavefront sensors (F-WFS, amongst which we notably find the Zernike WFS[3] and the pyramid WFS[4]). This bench aims at delivering a well-characterized and controlled environment to develop, test and compare F-WFS. Originally designed to work with a glass 4-faced pyramid prism, it recently evolved to a more complex setup, using a spatial light modulator (SLM[2]) in the focal plane to produce any kind of filtering phase mask. After a validation of the use of an SLM in the focal plane to produce F-WFS,[2] we noticed that the turbulence generator we were using at the time was (1) with fixed turbulence condition (i.e. r_0, L_0, wind speed, etc.) and (2) reproducing quite bad seeing conditions. We therefore decided to replace this phase screen with a second SLM, placed in the pupil plane and that serve as atmospheric turbulence generator as well as deformable mirror.

We present in this paper the upgrading and advances that have been made on the LOOPS bench in the last few months. After recalling the optical setup in Sec. 2, we present in Sec. 3 the work that has been done to calibrate the tip-tilt mirror and be able to produce precise and reliable modulation paths. Section 4 shows how we are now able, with only one SLM, to produce phase and amplitude at the same time in the pupil plane. Section 5 present the results obtained when trying to close the loop with n-faced pyramid WFS. And finally, Sec. 6 show the latest results on the characterization of different F-WFS.
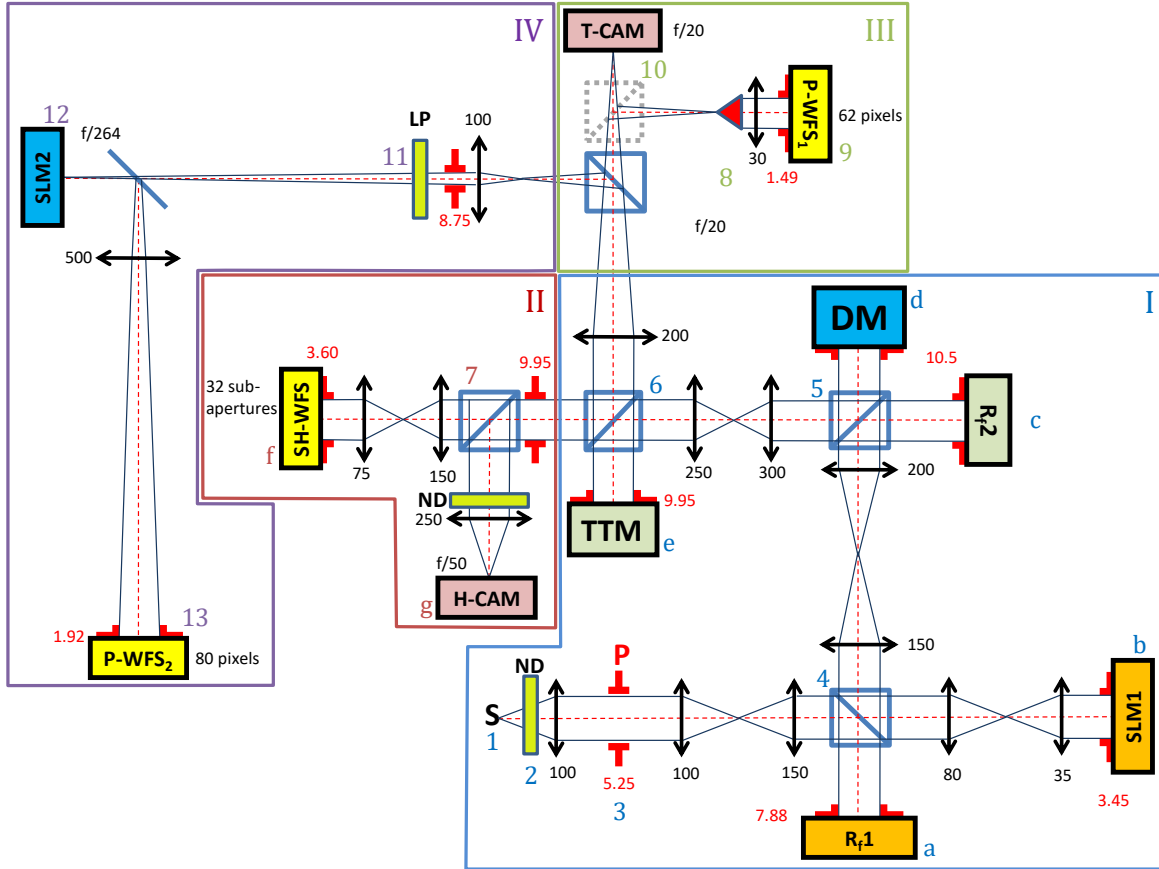
Figure 1: Schematic view of the LOOPS bench. Each pupil plane is marked with a red aperture and its physical diameter is given. The f# at the two cameras, pyramid and SLM positions are given as well. An animated demonstration of the working principle of the bench can be seen at https://youtu.be/lPOYgA9Amdo.

2. OPTICAL SETUP

The LOOPS bench has been designed to work as a modular adaptive optics facility. Figure 1 present the latest schematic of the bench. For a complete description of the optical setup, the reader can refer to the latest publication on the bench.[2] It includes, amongst other :

- a laser light source (marked as S on Fig. 1, $\lambda = 660$ nm),

- a pupil plane spatial light modulator (SLM1) serving at the same time as (1) a high resolution deformable mirror and (2) a turbulent phase screen generator. There are 320 pixel in the pupil diameter,

- an ALPAO deformable mirror (DM) with 9 actuators fitted into the pupil diameter,

- a tip-tilt modulation mirror (TTM) serving as the beam shaping tool, to produce modulation in the focal plane or simulate the observation of extended objects,

- a 32×32 Shack-Hartman (SH-WFS),

- a focal plane SLM (SLM2) used to produced any flavor of focal phase mask (n-faced pyramids, flatenned pyramid, Zernike WFS, etc.),

Further author information: (Send correspondence to P. Janin-Potiron)
P. Janin-Potiron: E-mail: pierre.janin-potiron@lam.fr, Telephone: +33 (0)4 91 05 59 59

- an OCAM^2 (P-WFS2) used as the pupil plane WFS camera.

Two focal plane cameras are also used to acquire focal plane images. One of them is affected by the modulation (T-CAM) while the other is not (H-CAM). Another OCAM^2 is available in the lab and is planned to be used to test real realisation of focal phase masks once they have been studied with the use of the SLM. Historically, this camera was the first to be used with a 4-faced pyramid on the LOOPS bench.[1]

3. MODULATION MIRROR CALIBRATION

The tip-tilt modulation mirror had to be calibrated in order to produce a reliable control of the modulation path. A function generator is used to control the x- and y-axis of the piezoelectric mirror. As Fig. 2 shows that (1) the x- and y-axis respond differently to a same excitation (in this case, a sine function with a 1.4V amplitude) and (2) the two directions adopted by the two axis are not orthogonal. After trying several calibration methods, we ended up using the most basic scheme. The calibration process is done as followed:

1. Define the voltage range on which to calibrate the mirror for the two axes,

2. Apply the voltage couple (v_1, v_2) on axes x and y respectively,

3. Measure the position (x, y) of the PSF in a focal plane,

4. Repeat step 2 and 3 for the whole range of voltage chosen in step 1,

5. Build the maps $v_1 = f(x, y)$ and $v_2 = f(x, y)$ as shown on Fig. 3.

Once done, we can finally reproduce any shape from a vector of coordinates (X, Y) (with $X = [x_0, x_1, ..., x_N]$ and $Y = [y_0, y_1, ..., y_N]$). We transform the path (X, Y) to its equivalent in the voltage space (V_1, V_2) from the maps obtained during the calibration stage. Finally, we apply this voltage vector to the function generator and send the commands to the tip-tilt mirror. We obtain images as presented on Fig. 4 where we produced rhodonea curves and one well-known sign in the focal plane by modulating the laser beam with tip-tilt in the pupil plane.
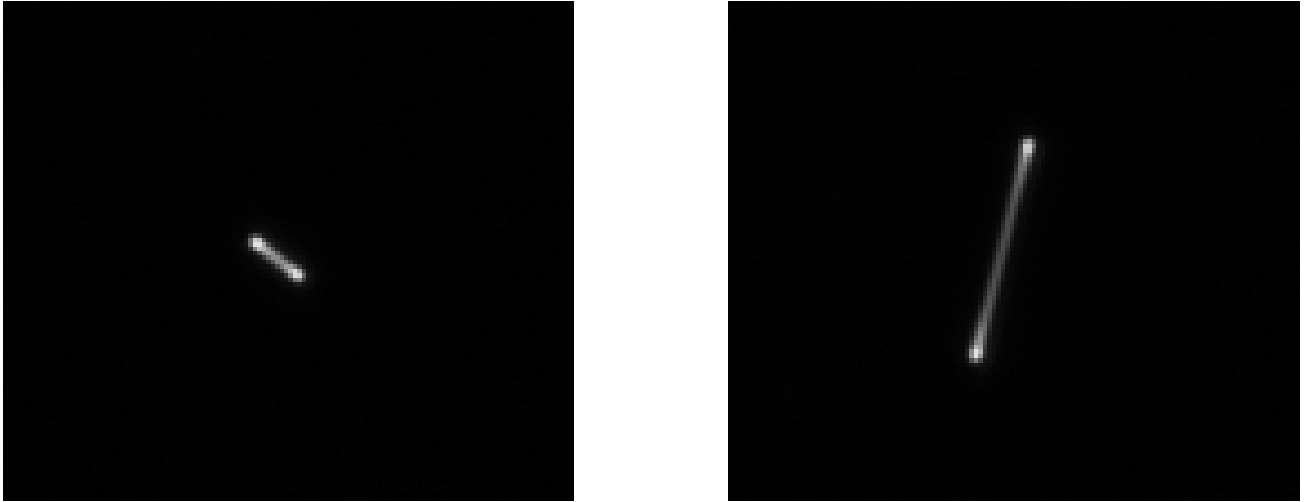

Figure 2: Modulation path when the tip-tilt mirror is excited with a sine function on its x-axis (left) and y-axis (right) with the same amplitude.
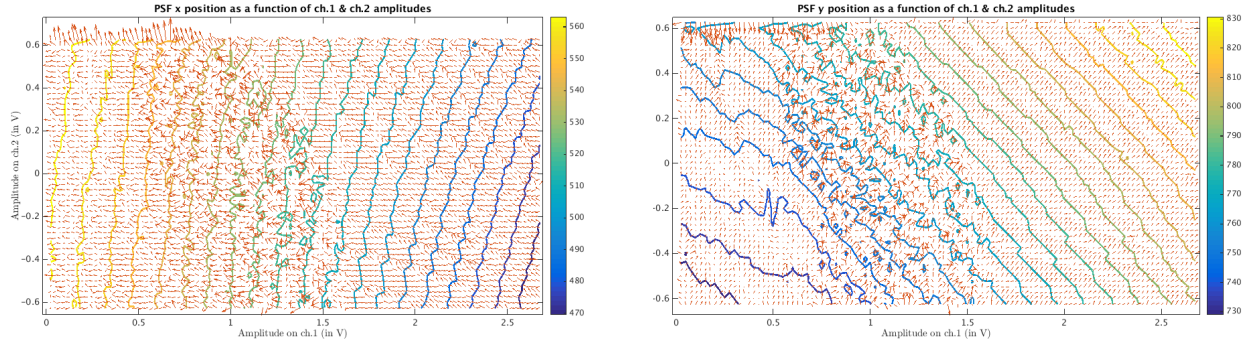
Figure 3: PSF x (left) and y (right) position as a function of the voltage on channels 1 and 2 of the tip-tilt modulation mirror.
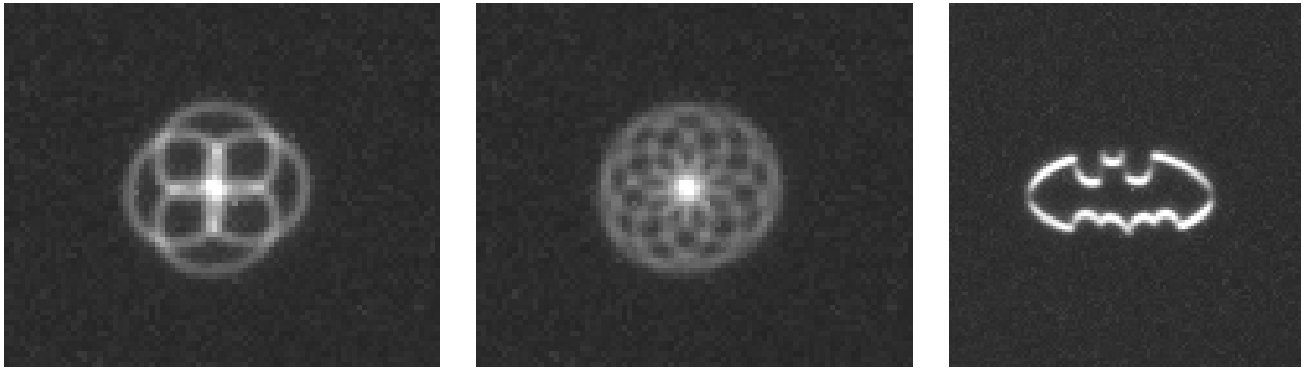

Figure 4: Modulation pattern created with the tip-tilt mirror.

4. AMPLITUDE AND PHASE CONTROL IN THE PUPIL PLANE

We work as well on applying amplitude masking in the pupil plane using the phase only SLM of the bench. Figure 5 show some results obtained when trying to apply amplitude mask on the pupil plane SLM. We don't show the contrasts curves here, but the ratio between light and dark zones of the image are typically lower than 1%. Obtaining these amplitude mask with a phase-only SLM require some work around that we briefly explain hereafter.
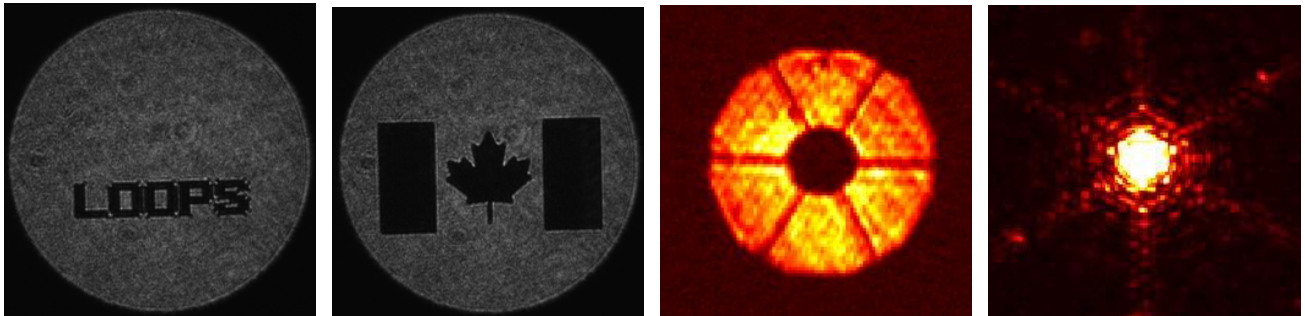

Figure 5: From left to right: (1,2) pupil images (LOOPS, Canada flag) taken in a relay pupil plane and demonstrating amplitude mask applied on the pupil plane SLM. (3) Pupil image taken with the OCAM in the WFS pupil plane and showing an ELT-like pupil mask produced on the pupil plane SLM. (4) PSF corresponding to the pupil in case (3). The diffraction effects from the spiders are clearly visible.
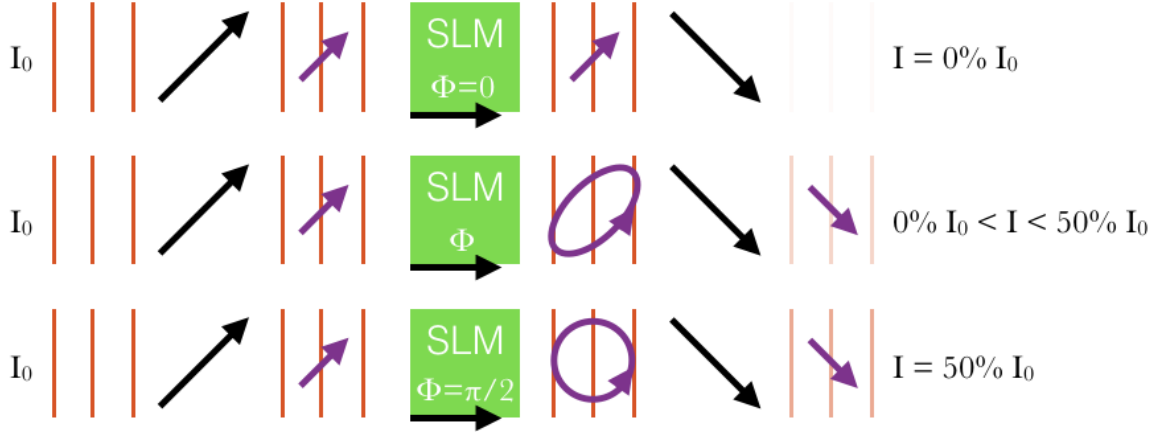
Figure 6: Explanation of how to produce amplitude modulation using phase only SLM and two crossed polarizers.

The technique we use to produce the images presented on Fig. 5 is based on applying tip-tilt on the region we want to cover in the pupil and filter the corresponding rejected light in the focal plane using a pinhole filter. This is a really convenient technic that is easily implemented and does not require any other resource or change on the bench.

A second way of doing the job would be to place the pupil plane SLM in between two crossed polarizer orientated respectively at $+45$ and -45 of the fast axis of the SLM's liquid crystals. Figure 6 is showing a scheme of the optical setup this technic would require. By adjusting the phase on the SLM, the $+45$ polarized light become an elliptically polarized light with its ellipticity depending on the phase (i.e. if (1) phase is 0 then the polarization is still linear, (2) phase is between 0 and $pi/2$ the polarization is elliptical and (3) phase is $pi/2$ then polarization is circular). When going through the second linear polarizer, the ligh is totally blocked in case (1), partially transmitted in case (2) and transmitted at 50% in case (3). This solution does not allow to produce amplitude and phase at the same time and is therefor not suitable for our application.

5. CLOSED-LOOP WITH N-FACED PYRAMIDS

After presenting the concept of the focal plane SLM in a previous publication[2] and demonstrating the closed-loop operation with a modulated 4-faced pyramid, it was time to play with some new WFS concept. We proposed to close the loop using 3-, 4-, 5-faced pyramids and an axicon. As the turbulent phase screen we were using at that time was introducing large aberrations on the wavefront, we modulated the beam at $5\lambda/D$ to extend the dynamic range of the sensors and be able to close the loop. Figure 7 shows a snapshot of the closed-loop regime for the four above mentionned WFS. A video showing the bootstrap sequence is available by following the link given in the description of Fig. 7.

6. FOURIER FILTERING WAVEFRONT SENSORS COMPARISON

Since the previous publication,[2] the bench has been upgraded with a second SLM put in a pupil plane (see Sec. 2). This device is intended to control the phase in the pupil plane, either to reproduce a DM AO correction, to introduce atmospheric turbulence or do both at the same time. The bench is controlled using OOMAO,[5] making it easy to transfer the experience from the simulation mode to the operation of the bench. Atmospheric turbulence is introduced on the bench using the *atmosphere* object from OOMAO. The DM is emulated using the *deformableMirror* object from OOMAO. It can be controlled in a zonal or modal fashion. For zonal control, the actuators influence function is produced using the *influenceFunction* object from OOMAO. For modal control, the modes can be either *Zernike*, *KL* or *Fourier*. It has been found that for high order correction (radial Zernike order around 12), the Zernike modes tend to introduce edge effects on the correction, therefor not being suitable for the closed-loop operation. That is why we are using the KL modes that don't exhibit this effect.
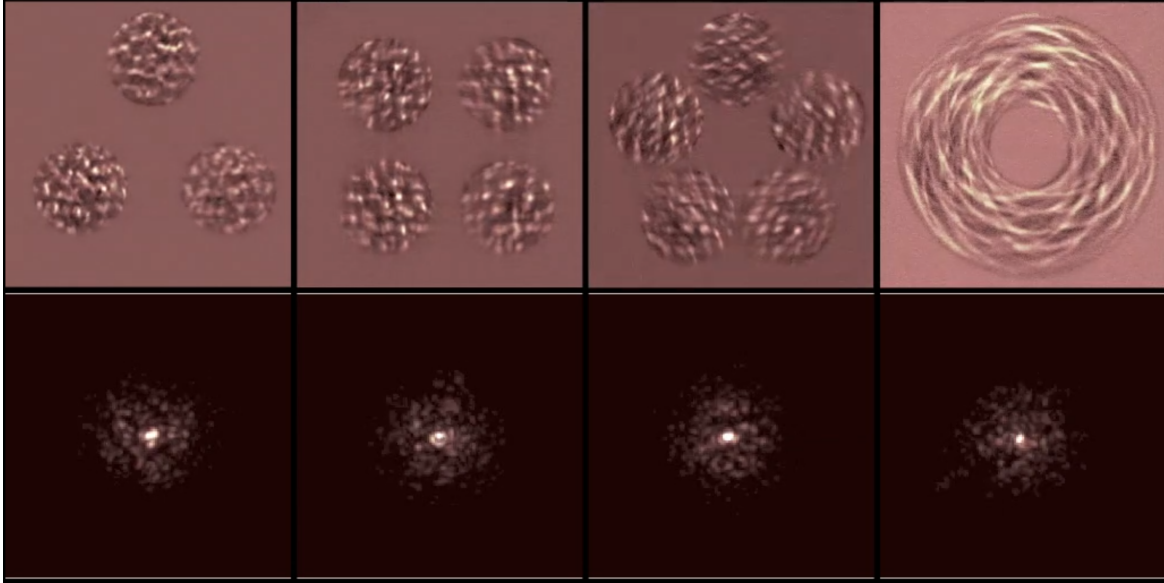
Figure 7: Closed-loop snapshot for (from left to right) the 3-, 4- 5-faced pyramid and an axicon. A video showing the bootstrap sequence is available at https://youtu.be/3mfKPwCKQ50

Using this new device we are now able to perform high resolution calibration and control of the system: (1) we can introduce Fourier modes onto the pupil and measure the optical transfer function of a given WFS in order to determine its sensitivity and dynamic, (2) we can choose the intensity of the phase aberration and close the loop with different WFS while completely mastering the turbulence that is seen be the WFS. These two points are treated briefly hereafter and will be the matter of next coming papers on the subject.

- Calibrating the system with pushing and pulling Fourier modes onto the pupil plane SLM, we are now able to measure the transfer function of the system for a given focal phase mask. We present on Fig.8 the results obtained for 6 different mask listed in the caption. The transfer function is derived from the interaction matrix D by calculating $TF = \sqrt{\mathrm{diag}(D^t D)}$. The min-max of the color axis is the same for each mask, making it direct to compare. For example, we se we retrieve the flat response expected for the Zernike WFS (bottom left) or the oscillating response of the flattened pyramid[6] (top right). This TF analysis allow us to infer the sensitivity of the WFS and therefor deduce their performances and compare them.

- We measured the r_0 values each WFS presented in Fig. 8 can tolerate and still be able to bootstrap. This parameter is giving a number that is directly driven by the dynamic of the WFS. Figure 9 presents the r_0 value for each WFS. The value is obtained by taking the mean of the tolerable r_0 on 10 random turbulence realisations, the realisation staying the same for the different mask. We can see that the 4-faced and 3-faced pyramid have the lowest limit r_0, meaning that they demonstrate the largest dynamic range. From the other side, we retrieve the Zernike WFS and it's well known low capture range, limited from $-\lambda/4$ to $\lambda/4$. Increasing the number of random starting screen would certainly help to be more confident in the data we obtained.

- We describe in Sec. 6 the change we made to the bench by replacing the turbulent rotating phase screen by a second SLM. This allowed us to be able to control the amplitude of the phase aberrations we put in the pupil plane and to close the loop with sensors that present reduced dynamic range compared to the ones presented in Fig. 7. We therefore created a flattened pyramid WFS[6] onto the focal plane SLM and close the loop. Figure 10 shows a snapshot of the closed-loop operation of the flattened pyramid. We see on the extreme right of the figure the long exposure PSF (simulated by Fourier transform of the phase residuals applied to the SLM) that demonstrate a relatively good correction.
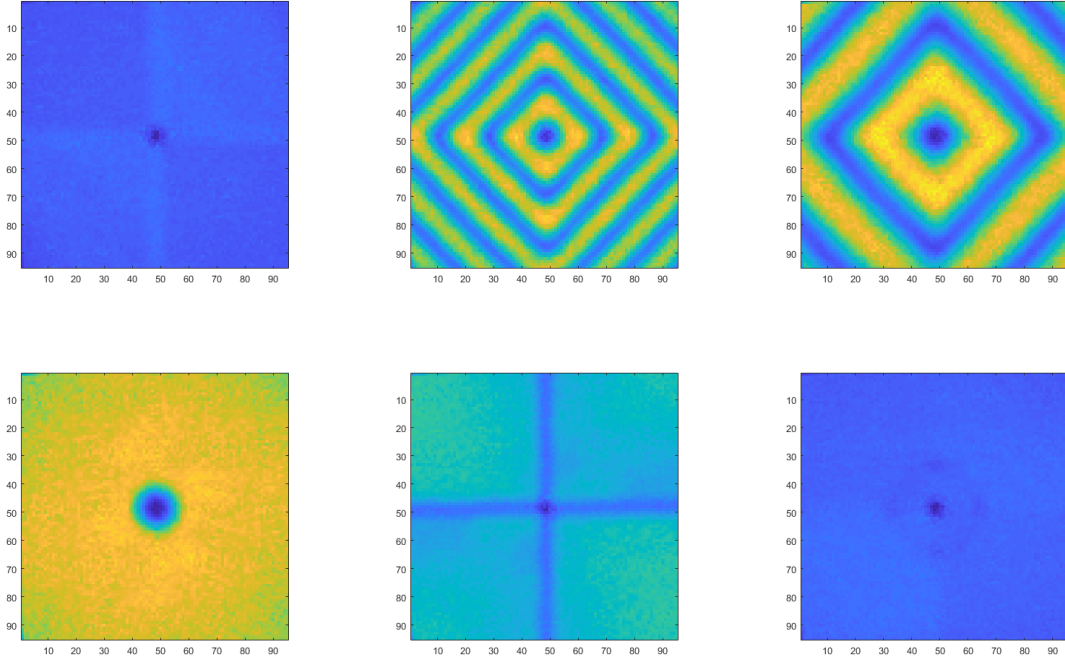
Figure 8: Transfer function measured on the LOOPS bench for different mask. From top left to bottom right: 4-faced pyramid, 4-faced flattened pyramid with $0.3D$ center-to-center separation, 4-faced flattened pyramid with $0.15D$ center-to-center separation, ZELDA, iQuad,[7] Hybrid-WFS (saw at the conference, credits to R. Holzlöhner *et al.*).
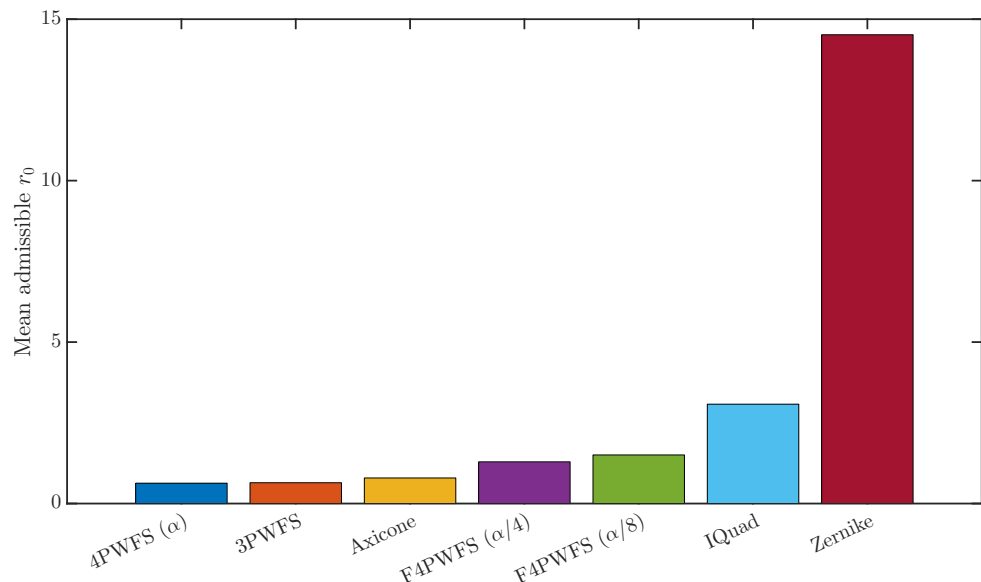

Figure 9: Mean acceptable r_0 value for bootstrap operation for different focal phase masks.

7. CONCLUSION

We showed in this paper the latest advances that have been made on the LOOPS bench since the last publication. The integration of a second SLM, placed in a pupil plane, is the major change and is opening a powerful way of controlling the bench. Being able to introduce high resolution phase screens in the pupil, either to introduce
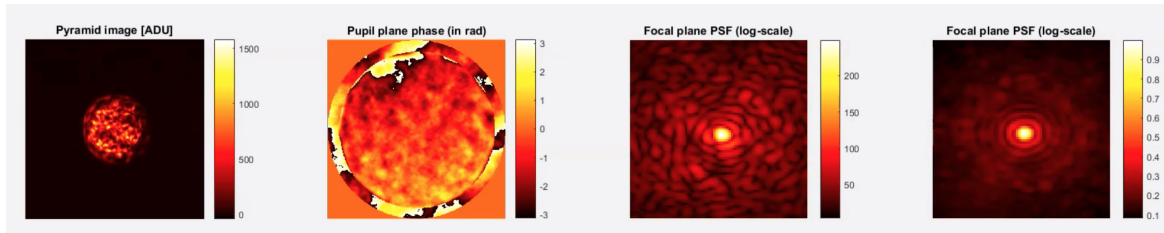
Figure 10: Closed-loop data taken from the bench using a 4-faced flattened pyramid. From left to right: WFS pupil plane image, phase applied on the pupil plane SLM (in rad), short exposure PSF and long exposure PSF. The PSF are simulated using fast Fourier transform of the SLM phase in the pupil plane. Animation of the open to closed loop transition is visible at https://youtu.be/BbEnV1DqdhA.

turbulence or mimic the action of a DM is a huge improvement. We demonstrated as well that we are able to produce amplitude masking with the same device, opening the path to the study of petaling effects that have been found in simulations reproducing the E-ELT operation.

The most important study that is currently on-going is the comparison of different F-WFS to try to classify their performances and develop a standard method to rank their performances depending o the application that are foreseen. Sensitivity and dynamic measurements have been made and remained to be associated with their respective closed-loop performance. The advances made on the optical gain will also be integrated on the bench (see the proceding from Chambouleyron *et al.*).

Other projects, such as testing the INGOT WFS (see the proceeding from Di Filippo *et al.*) are currently on-going and will surely provide interesting results in the comming months.

Funding

REFERENCES

[1] C. Bond, K. El Hadi, J. F. Sauvage, *et al.*, "Experimental implementation of a Pyramid WFS: Towards the first SCAO systems for E-ELT," in *Adaptive Optics for Extremely Large Telescopes IV (AO4ELT4)*, E6 (2015).

[2] P. Janin-Potiron, V. Chambouleyron, L. Schatz, *et al.*, "Adaptive optics with programmable Fourier-based wavefront sensors: a spatial light modulator approach to the LAM/ONERA on-sky pyramid sensor testbed," *Journal of Astronomical Telescopes, Instruments, and Systems* **5**(3), 1 – 10 (2019).

[3] M. N'Diaye, A. Vigan, K. Dohlen, *et al.*, "Calibration of quasi-static aberrations in exoplanet direct-imaging instruments with a Zernike phase-mask sensor. II. Concept validation with ZELDA on VLT/SPHERE," *A&A* **592**, A79 (2016).

[4] R. Ragazzoni, "Pupil plane wavefront sensing with an oscillating prism," *Journal of Modern Optics* **43**(2), 289–293 (1996).

[5] R. Conan and C. Correia, "Object-oriented Matlab adaptive optics toolbox," in *Adaptive Optics Systems IV*, E. Marchetti, L. M. Close, and J.-P. Vran, Eds., **9148**, 2066 – 2082, International Society for Optics and Photonics, SPIE (2014).

[6] O. Fauvarque, B. Neichel, T. Fusco, *et al.*, "General formalism for Fourier-based wave front sensing: application to the pyramid wave front sensors," *Journal of Astronomical Telescopes, Instruments, and Systems* **3**, 019001 (2017).

[7] O. Fauvarque, P. Janin-Potiron, V. Hutterer, *et al.*, "*i*Quad wavefront sensor," (2019 - in prep.).